PCCP

First Principles Analysis of Surface Dependent Segregation in Bimetallic Alloys

Journal:	*Physical Chemistry Chemical Physics*
Manuscript ID	CP-ART-07-2019-003984.R1
Article Type:	Paper
Date Submitted by the Author:	25-Sep-2019
Complete List of Authors:	Farsi, Lida; Worcester Polytechnic Institute, Chemical Engineering Deskins, Nathaniel; Worcester Polytechnic Institute, Chemical Engineering

First Principles Analysis of Surface Dependent Segregation in Bimetallic Alloys

Lida Farsi, N. Aaron Deskins*

Department of Chemical Engineering

Worcester Polytechnic Institute, Worcester MA 01609

*nadeskins@wpi.edu

Abstract

Stability is an important aspect of alloys, and proposed alloys may be unstable due to unfavorable atomic interactions. Segregation of an alloy may occur preferentially at specific exposed surfaces, which could affect the alloy's structure since certain surfaces may become enriched in certain elements. Using density functional theory (DFT), we modeled surface segregation in bimetallic alloys involving all transition metals doped in Pt, Pd, Ir, and Rh. We not only modeled common (111) surfaces of such alloys, but we also modeled (100), (110), and (210) facets of such alloys. We showed that segregation is more preferred for middle transition metals, with early and late transition metals being most stable within the parent metal. We find these general trends in segregation energies for the parent metals: Pt > Rh > Pd > Ir. A comparison of different surfaces suggests no consistent trends across the different parent hosts, but segregation energies can vary up to 1.5 eV depending on the exposed surface. We also developed a statistical model to predict surface-dependent segregation energies. Our model is able to distinguish segregation at different surfaces (as opposed to generic segregation common in previous models), and agrees well with the DFT data. The present study provides valuable information about surface-dependent segregation and helps explain why certain alloy structures occur (e.g. core-shell).

1. Introduction

Platinum group metals, such as Pt, Pd, Rh, and Ir often display high catalytic activity for catalytic reactions. These metals can be expensive, so alloys are often used to decrease the amount of expensive metal being used, while also achieving high catalytic activity. Alloys have been investigated for instance in hydrogen generation[1,2], dehydrogenation[3-5], reforming processes[6,7], and fuel cells[8-11]. In order to design viable alloy catalysts, the materials should have high catalytic activity, but should also be stable. Depending on how well the two metals mix, different alloy structures may form[12]. For instance, an alloy may form a homogenous structure for metals that mix

well, while separation into distinct particles or core-shell particles may occur for metals that prefer to segregate.

Surface segregation leads to the surface of an alloy particle/crystal having a different alloy composition than the bulk. Surface segregation can influence many processes such as adsorption, wetting, crystal growth, oxidation, corrosion, and catalysis[13,14]. Several tools, computational and experimental, can be used to study and identify alloy segregation[15]. Depending on the application of interest, surface segregation can be beneficial or detrimental[16,17]. For instance, segregation of Pt atoms to the surface of a $Pt_{75}Ni_{25}$ alloy enhanced the catalytic activity for the oxygen reduction reaction (ORR).[18-20] On the other hand, possible segregation of an element M in M (core)-Pt (shell) structures may decrease the stability of these alloys in acidic medium[21,16]. Different parameters have been used to explain surface segregation. Atom size and surface energy difference between the host metal and the impurity element have been investigated[22,16,23]. Elastic energy release[24], heat of solution for the alloy[24], composition of the elements in the alloy[16], and cohesive energy[23] are other properties tied to surface segregation.

Thermodynamics may drive what type of structure forms in an alloy (or nanoalloy for nanoparticles), and modeling can be used to predict such structures[25]. Segregation has already been studied in previous reports using tools such as density functional theory (DFT). Ruban et al[26-28] for instance calculated segregation energies of single impurity atoms in several low-index surfaces[26-28]. Segregation behavior for the (111) surfaces of platinum[16,29,30], palladium[22,31,32], and iridium[21] has been investigated. Segregation behavior can be surface dependent, meaning that it can depend on what surface is exposed. Ruban et al.[28] reported that the segregation energy is related to the nature of d-bands which vary across the different transition metals. Other DFT work that indicates that the core metal in core/shell structures can affect surface adsorption, and choice of core determines alloy stability[33]. Other work modeling Pt_3M alloys shows that metal choice M affects alloy segregation and surface reactivity for the oxygen reduction reaction[34]. Surface segregation at the (111)[20, 35-42], (110)[20, 35-38, 40-42], and (100)[20, 35-43] surfaces of Pt has been studied. Surface segregation at the (111)[38, 44-46], (110)[38,45,46], and (100)[38, 43-46] surfaces of Pd has also been investigated. Besides DFT, other models have been developed to predict alloy structures, such as coordination-dependent models to predict structure and segregation in a Pt-Pd particle and Pt-Rh(111) surface[39], or other bimetallic surfaces/particles[47].

Such studies have shown that segregation behavior could occur differently at various surfaces. A potential shortcoming in existing studies is the limited number of impurities that have been considered. For instance, several of these studies only considered binary Pt-Ni[20, 35, 36, 40, 42] and Pt-Pd[44-46] alloys. The segregation energy, a measure of how much an impurity element prefers to segregate from a parent element, can be a good indicator of the alloy's stability[22,21]. While published literature has determined segregation energies for select metals in select surfaces, a comparison of many different surface facets (e.g. open and closed) is not currently available. Furthermore, the most comprehensive collection[27, 28] of segregation energies in the literature uses the local density approximation (LDA), while in the present study, we performed DFT calculations using generalized gradient approximation (GGA) functionals, which are more common for modeling metals.

We have performed a systematic study of the (111), (110), (100), and (210) surfaces using Pt, Pd, Rh, and Ir as host metals. We considered all transition metals as dopants, and investigated how segregation compares for the different surface facets. It is important to note that segregation energy also depends on the alloy's composition and depending on how many atoms are being segregated, different segregation energies can be obtained. In the present study, we considered dilute alloys, specifically we modeled a single impurity (dopant) in the host metal. We also addressed how different types of segregation (sub-surface to surface versus bulk to surface) affect segregation energy results. Finally, we presented models that may explain these surface segregation processes, and can be used to make predictions of alloy segregation.

2. Methodology

2.1. Simulation Parameters

Density functional theory (DFT) calculations were performed using the CP2K package[48-52] which uses the Gaussian and plane waves (GPW) method[50]. Electron densities were treated by plane waves and electronic orbitals were treated by double-zeta Gaussian basis sets.[53] Core electrons were represented by Goedecker-Teter-Hutter (GTH) pseudopotentials[54,55]. All calculations were spin-polarized. CP2K uses periodic boundary conditions and samples reciprocal space only at the Γ point. To compensate for any error associated with small k-point sampling, large cells have been used. We performed several calculations to assess the effect of using different parameters for the calculations, and discuss this in more detail in the Supporting Information.

These calculations indicate that the chosen parameters (cell size, exchange correlation functional, basis set) are adequate for the current study. We also used similar simulation parameters in our previous work[56], where we showed the approach to give similar results to common DFT plane wave calculations.

The Perdew, Burke, and Ernzerhof (PBE) exchange correlation functional[57] was used throughout the present study. A shortcoming of this functional is that other less-common functionals may give slightly better surface energies or lattice parameters[58]. Other methods, such as based on wavefunctions rather than electron density, may also give better descriptions[59] (albeit at increased computational time). Nonetheless DFT and the PBE functional has been used widely to model metal systems because they provide reasonable accuracy[60, 61] without protracted computational times.

2.2. Surface Models

In order to build surfaces, first we calculated lattice parameters of bulk metals that were used as alloy hosts: 3.86 Å (Ir), 3.96 Å (Pt), 3.95 Å (Pd), and 3.84 Å (Rh). These values match well with other density functional theory studies: 3.86 to 3.89 Å for Ir[62, 63], 3.99 Å for Pt[63, 64], 3.93-3.96 Å for Pd[63, 65-69], and 3.80 Å to 3.86 Å for Rh[63, 70-72]. Next we modeled surfaces using periodic boundary conditions, or the slab approach. For (111) and (100) surfaces, 6×6 super cells were used. Both (111) and (100) surfaces were 5 atomic layers thick consisting of 180 atoms. For (110) surfaces, 4×6 super cells with 7 atomic layers consisting of 168 atoms were used. For (210) surfaces, 2×4 supercells with 5 atomic layers consisting of 160 atoms were used. All atoms were allowed to relax for the various slabs. The corresponding slab models are depicted in Figure 1. We investigated how the number of layers affected our results. We also examined how freezing the bottom layers compared to not freezing the bottom layers affected our results. We discuss these aspects in the Supporting Information.

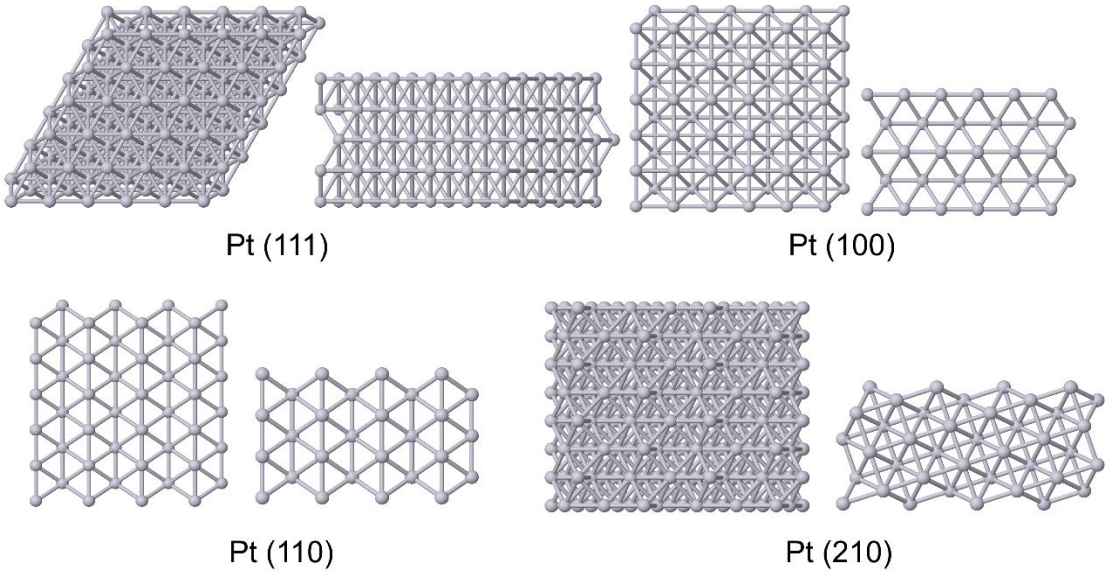

Figure 1. Slab models used in the present study. For each surface, the left image shows the top view of the surface, while the right image shows the side view of the surface.

2.3. Segregation definition

In order to model segregation, we considered a dopant atom in the first (top) surface layer, in a sub-surface layer, or in a larger bulk structure. The bulk structure was of size 5 × 5 × 5 and had 500 atoms. The dopant atom may transfer from the sub-surface layer to the first surface layer, or from the bulk to the first surface. Both segregation processes were considered in this work. The positions of a dopant in the alloy for the (111) surface and bulk are depicted in Figure 2. We show other dopant positions in Figure S1. There are several possible sub-surface sites that could be considered, but we modeled those depicted in Figure S1. The segregation energy, $E_{seg-1-sub}$, is defined as the total energy difference of the alloy with dopant in the first layer and sub-layer. An alternative definition, $E_{seg-1-bulk}$, is defined as the total energy difference of the alloy with dopant in the first layer and bulk structure. The segregation energy is calculated by Equations (1) and (2):

$$E_{seg-1-sub} = E_{1st\ layer} - E_{sub\ layer} \quad (1)$$

$$E_{seg-1-bulk} = E_{pure\ bulk} + E_{1st\ layer} - E_{impurity\ in\ bulk} - E_{pure\ surface} \quad (2)$$

In these equations E_{seg} is the calculated segregation energy, $E_{1st\ layer}$ is the total energy of the alloy with the dopant in the first layer, and $E_{sub\ layer}$ is the total energy of the alloy with the dopant in the sub-layer. The bulk energies, $E_{pure\ bulk}$ and $E_{impurity\ in\ bulk}$, are the total energies of a dopant-free bulk cell and the bulk structure with a single atom dopant. A negative segregation energy indicates that the dopant prefers to segregate towards the surface, while positive segregation energy indicates the dopant does not prefer to segregate towards the surface. Unless noted in the text, when we refer to segregation energy, this indicates the $E_{seg-1-bulk}$ value. We also mention that we only focus on the thermodynamics of segregation in this paper. Certainly kinetics may play an important role in hindering the segregation of two metals, but addressing kinetics is beyond the scope of the current paper.

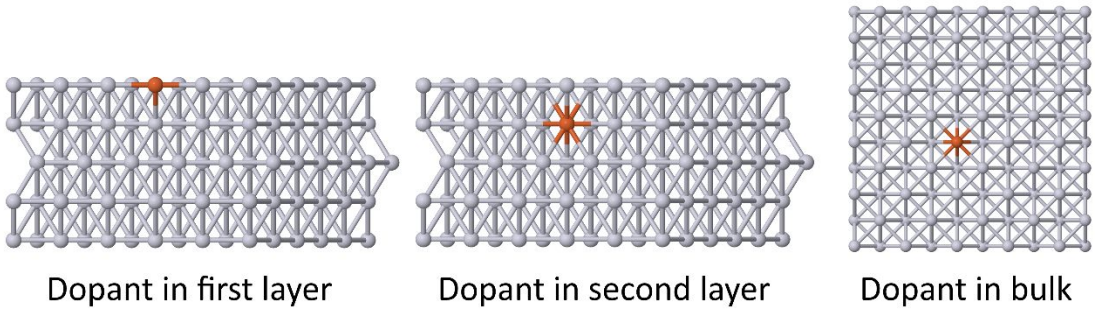

Figure 2. Illustration of different dopant positions within parent metals in slab and bulk structures. Side views of the slabs and bulk are shown.

3. Results and discussion

3.1. Comparison of Segregation on (111) Surfaces

We first examined segregation of transition metals at the (111) surfaces. Calculated segregation energies ($E_{seg-1-bulk}$) are given in Figure 3. The segregation energy curves have a characteristic U shape, where early and late transition metals have the most negative segregation energies while middle transition metals have the most positive segregation energies. This is similar to previous work, such as Ruban et al[28], Chelikowsky[73], and Mukherjee et al[74]. However, there is anomalous segregation behavior for 3d metals, especially middle metals like Cr, Mn, and Fe. The segregation energy curve for the 3d metals does not have a full U shape, but rather dips for the middle transition metals, in contrast to the 4d and 5d metals. A similar anomalous dip was

predicted by others[28]. 3d metals have anomalous behavior compared to 4d and 5d, due to stronger magnetic effects arising from narrow d bands[75]. This dip for mid transition metals occurring in the 3d row can be observed for other properties, such as surface enthalpy[73] or DFT-calculated cohesive energies (which agree well with experimental cohesive energies also showing this dip)[76]. DFT may not be able to fully describe such magnetic effects, and multireference methods may be need to better describe such metals, but DFT is able to reasonably capture these magnetic effects[77]. Our results for 3d metals are consistent with experimental work showing that middle 3d metals display anomalous behavior compared to 4d and 5d metals.

We calculated the average segregation energies in the different host metals Pt, Pd, Ir, and Rh to be 0.99, 0.52, -0.24, and 0.55 eV, respectively. Ranges of segregation energies in the host metals were as follows: Pt (-0.77 to 2.26 eV), Pd (-0.56 to 1.97 eV), Ir (-3.10 to 1.30 eV), and Rh (-1.40 to 2.15 eV). The segregation energies in general follow this trend: Pt > Rh > Pd> Ir for 4d and 5d dopants. That is, the segregation energies in the Pt (111) surface tend to be most positive, while the segregation energies in the Ir (111) surface tend to be most negative. Thus, segregation is least likely to occur within Pt and most likely to occur within Ir. For 3d transition metals however, Pd and Ir possess the least segregation energy values among other hosts. Due to oscillatory behavior of surface segregation in 3d transition metals, it is hard to report a monotonic segregation trend as was done for 4d and 5d dopants.

One factor affecting surface segregation is the metal atomic size. When the dopant atom is bigger than the host metal, strain occurs. In order for this strain to be released, the dopant could segregate to the surface and leave the metal lattice. For a given dopant, the bigger the host metal, the less likely segregation occurs due to strain. Pt has the largest van der Waals radius among the four host metals, while Rh and Ir have the smallest radii. As a result, surface segregation is least likely to occur in Pt, and more likely to occur in other hosts. As we show in section 3.e, there are also other factors affecting surface segregation. Therefore, our results cannot be interpreted merely by metal atomic size.

As can be seen in Figure 3, segregation energies are most negative for early and late transition metals and most positive for the middle transition metals. In other words, early and late transition metals are most likely to segregate from the parent metal. Chelikowsky et al.[73] used Miedema[78] theory to examine such trends. Chelikowsky showed that the segregation energy is

proportional to the cohesive energy of the metal. As discussed by Sutton[75], a transition metal's cohesive energy can be estimated from the number of d electrons (n_d) based on a Friedel model approximation. The maximum cohesive energy occurs for when $n_d = 5$, or for middle transition metals. Thus, middle transition metals have the largest cohesive energies and correspondingly the largest segregation energies. Brejnak and Modrak[79] attempted to explain segregation based on number of d electrons, and suggest that for host metals with $n_{d\text{-host}} > 5$, segregation will occur when $n_{d\text{-dopant}} > n_{d\text{-host}}$. We do observe favorable segregation for metals having $n_{d\text{-dopant}} > n_{d\text{-host}}$, as seen in Figure 3, but favorable segregation also occurs for some early transition metals, in contrast to the predictions of Brejnak and Modrak[79].

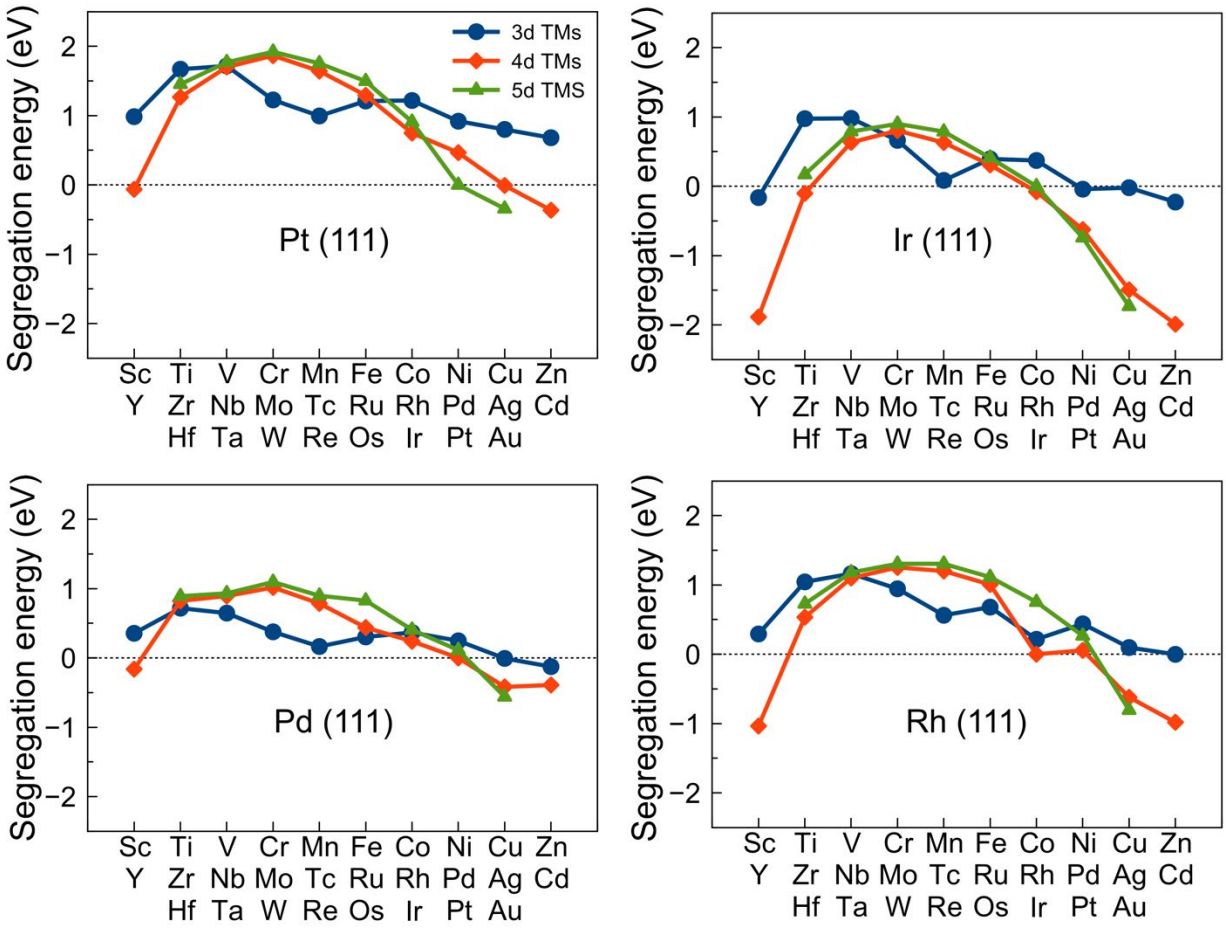

Figure 3. Calculated segregation energies ($E_{seg-1-bulk}$) of single transition metal atoms within the (111) surfaces of Pt, Pd, Ir, and Rh.

3.2. Comparison of Segregation in the (111), (100), (110), and (210) Surfaces of Pt

Surface segregation can be surface dependent, meaning that it may depend on what parent surface the segregation is occurring at. For instance, Duan et al.[45] studied surface segregation with Pt-Pd alloyed nanoparticles and observed different segregation tendencies for (100), (110) and (111) surfaces of these particles. To demonstrate this point, we show surface segregation energies for Pt (111), (100), (110), and (210) surfaces in Figure 4. For some dopants, there is a large segregation energy difference between the Pt surfaces. For instance, several dopants (e.g. Co, Ti, V, Sc) have large segregation energy differences (0.9 to 0.6 eV) between the (110) and (100) surfaces. In general the lowest segregation energies occur for the (110) surface, while the highest segregation energies occur for the (100) surface. Other metals (e.g. Pd, Os, Ir, Au) have much smaller differences ($\approx$ 0.1 eV) between the (110) and (100) surfaces. The average segregation energies are 1.2, 1.1, 1.0, and 0.7 eV for the Pt (100), (111), (210), and (110) surfaces, respectively, or (100) > (111) > (210) > (110).

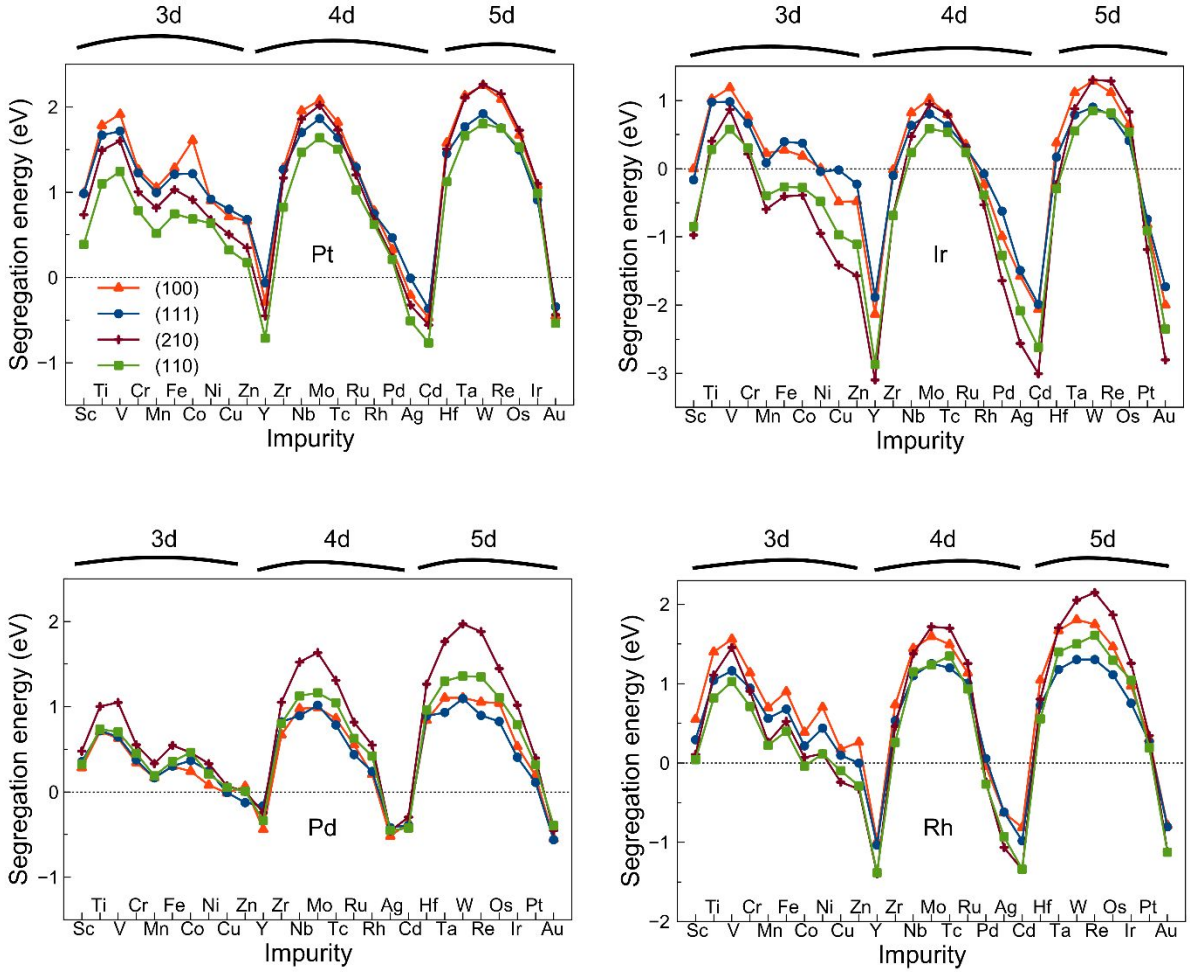

Figure 4. Segregation energy ($E_{seg-1-bulk}$) comparisons between difference surfaces of Pt, Ir, Pd, and Rh.

An examination of the different dopant metals provides details on segregation. Surface-dependent segregation is most pronounced for the 3d transition metals. The average segregation energy difference between (100) and (110) surfaces for 3d metals was calculated to be 0.6 eV. The average segregation energy differences between (100) and (110) surfaces for 4d and 5d transition metals was calculated to be 0.3 eV for both cases. The relative order of segregation energies across the various surfaces were different for the 3d, 4d, and 5d metals. For 3d metals the segregation

energies were generally as follows: (100) > (111) > (210) > (110). For a few later transition metals (Ni, Cu, Zn), however, the (111) segregation energies are higher than the (100) segregation energies. The segregation energies of many middle 4d and 5d transition metals follow this trend: (100) ≈ (210) > (111) > (110). For early and late transition 4d and 5d metals, however the segregation energies across the different surfaces become closer, and it becomes difficult to distinguish surface-dependent segregation. For instance, segregation energies of 5d metals for the (100) and (210) surfaces are very close, with a mean absolute difference of 0.04 eV between the two surfaces. Of note is that segregation energies with 4d and 5d metals have a much greater range (-0.8 to 2.3 eV) than the range of the 3d segregation energies (0.2 to 1.9 eV). 3d metals behave differently than 4d and 5d metals due to their unique magnetic properties as discussed before[75].

3.3. Surface Segregation in Pt, Ir, Pd, and Rh

Segregation energy comparisons between different surfaces of Pt, Ir, Pd, and Rh are shown in Figure 4. In the case of Pt and Pd as host, segregation energies for (111), (100), (110), and (210) surfaces converged to almost the same value at the start and the end of the transition metal series. For Ir and Rh, this is not the case and for Ir as host, and the values of segregation energies at the beginning and the end of transition metals differ the most for (111), (100), (110), and (210) surfaces (compared with Pt, Pd, and Rh as hosts). The segregation energies with Ir as host are between -3.10 and 1.30 eV. The corresponding ranges for Pt, Pd, and Rh surfaces as hosts are -0.77 to 2.26, -0.56 to 1.97, and -1.40 to 2.15 eV, respectively. The most positive segregation energies occurred with Pt as the host. Pt had the highest segregation energy, at 2.26 eV for W in the (210) surface. The lowest segregation energy value occurred with Ir, at -3.10 eV for Y in the (210) surface. The average segregation energies for Pt, Ir, Pd, and Rh are 0.99, -0.24, 0.52, and 0.55 eV, respectively. The segregation energy trends are thus roughly Pt > Rh > Pd > Ir when considering all the (111), (100), (110), and (210) surfaces. Full results for the (111) surfaces are shown in Figure S5 in the SI.

As evident from Figure 4, segregation energies appear to be surface dependent. For Pt and Ir as host, the 3d dopant segregation energies depended strongly on the surface, meaning that there is up to 1.4 eV energy difference between segregation of 3d dopants when different facets occur in the parent Ir or Pt metals. In the case of Pd as a host, there is up to a 1.0 eV energy difference

in segregation for 4d and 5d dopants within different facets of Pd. For Rh as host the surface dependent segregation is most pronounced for 5d transition metals with about an 0.8 eV energy difference between difference facets. From Figure 4 it can be observed that there is not a consistent trend in preferred surface dependent segregation. For example, with Pt as host and 3d transition metals as dopants the segregation energies follow this trend: (100) > (111) > (210) > (110). On the other hand with Rh as host and 5d transition metals as dopants this trend occurs: (210) > (100) > (110) > (111). In some cases, such as Pd as host and 3d transition metals as dopants, there is not an obvious trend in surface dependent segregation energy. In order to further explain such trends, we have developed a model to predict surface dependent segregation energies, as discussed in Section 3.5.

3.4. Bulk versus Sub-Layer Segregation

We next address segregation from sub-surface sites to the surface compared to segregation from the bulk to surface. Both processes have been studied in the literature[16, 22, 24, 28]. Figure 5 shows the calculated segregation energies using Equation (1) (sub-surface to surface segregation) and Equation (2) (bulk to surface segregation) with Pt as the host. A clear trend in the results is that sub-surface segregation energies are lower than bulk segregation energies, indicating that bulk segregation is harder. This would suggest that as the dopant metal gets closer and closer to the surface, it becomes less stable relative to the bulk, until at the surface it may or may not reach a stable state. The plots all have similar shapes indicating that the segregation energies are largely just shifted relative to each other. The mean absolute differences between bulk and sub-surface segregation energies are 0.49 eV (111), 0.54 eV (100), 0.60 eV (110), and 0.82 eV (210), with standard deviations of 0.35 eV (111), 0.38 eV (100), 0.42 eV (110), and 0.58 eV (210). The corresponding graphs for Ir, Pd, and Rh as hosts are depicted in Figures 6-8. For Ir and Pd as host, the two segregation processes have similar segregation energies, as evident in Figures 6 and 7. The mean absolute difference between bulk and sub-surface segregation energies for Ir was 0.24 eV, while the similar value for Pd was 0.13 eV. The differences are more noticeable for Rh (Figure 8), but the trends are similar between the two segregation processes.

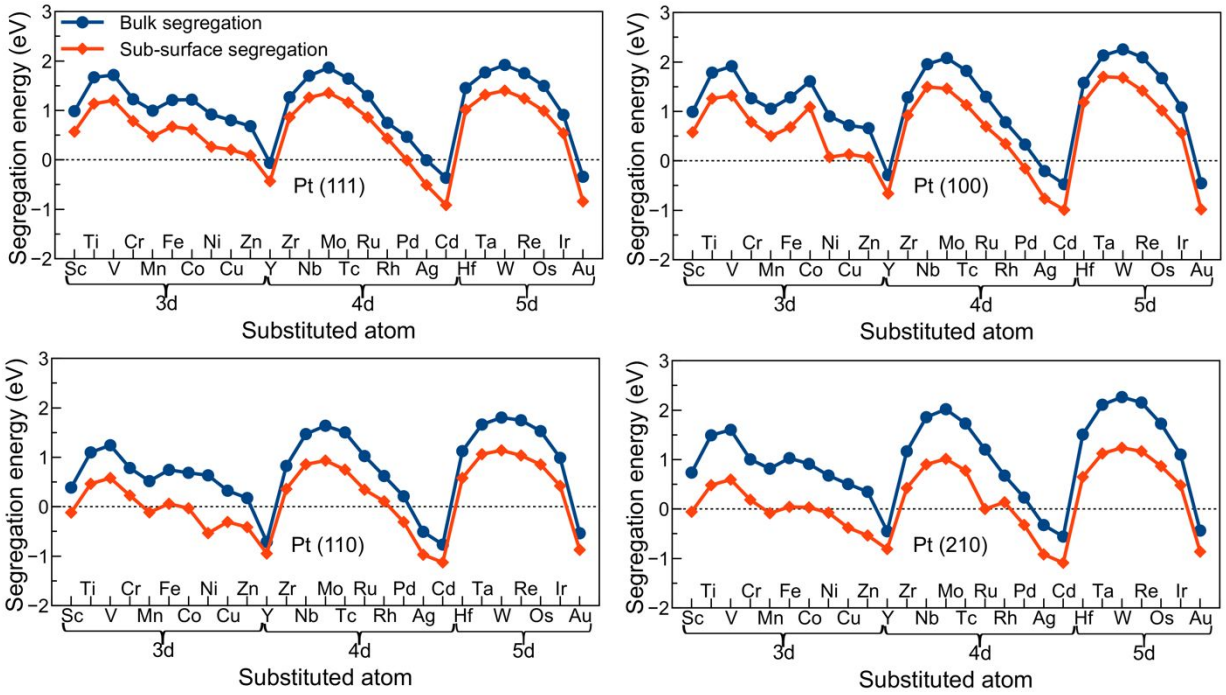

Figure 5. Calculated segregation energies in a Pt host metal involving sub-surface to surface segregation and also bulk to surface segregation. Segregation energies were calculated with Equations (1) and (2).

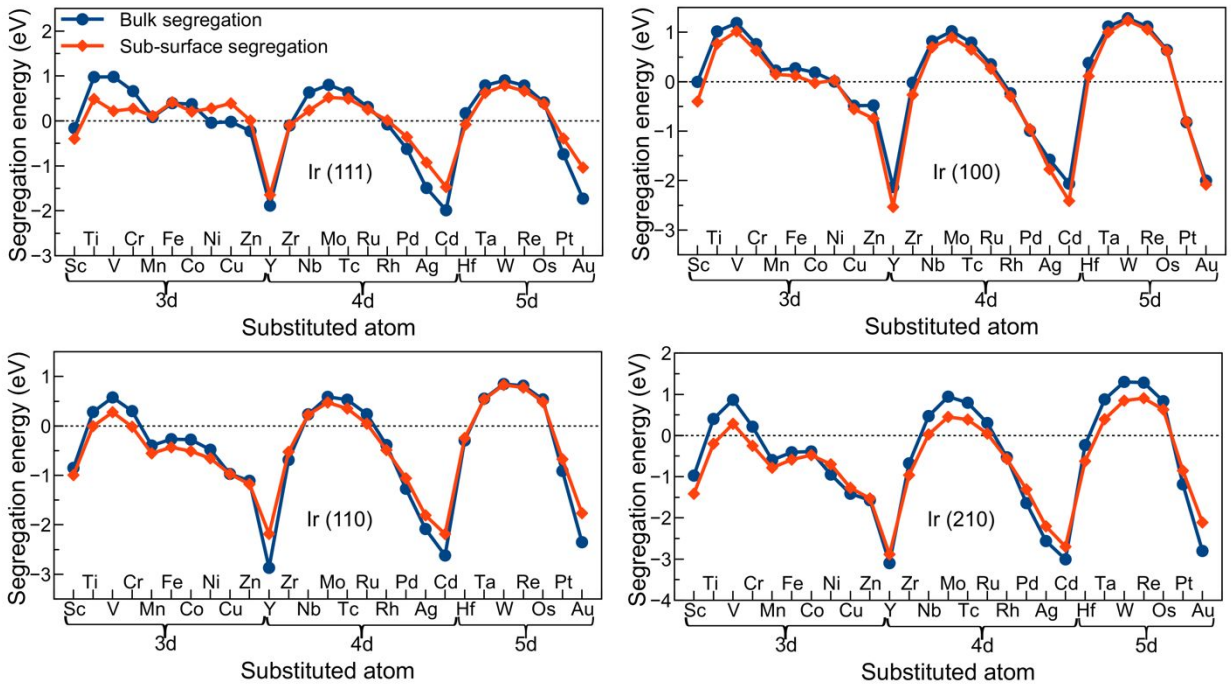

Figure 6. Calculated segregation energies in a Ir host metal involving sub-surface to surface segregation and also bulk to surface segregation. Segregation energies were calculated with Equations (1) and (2).

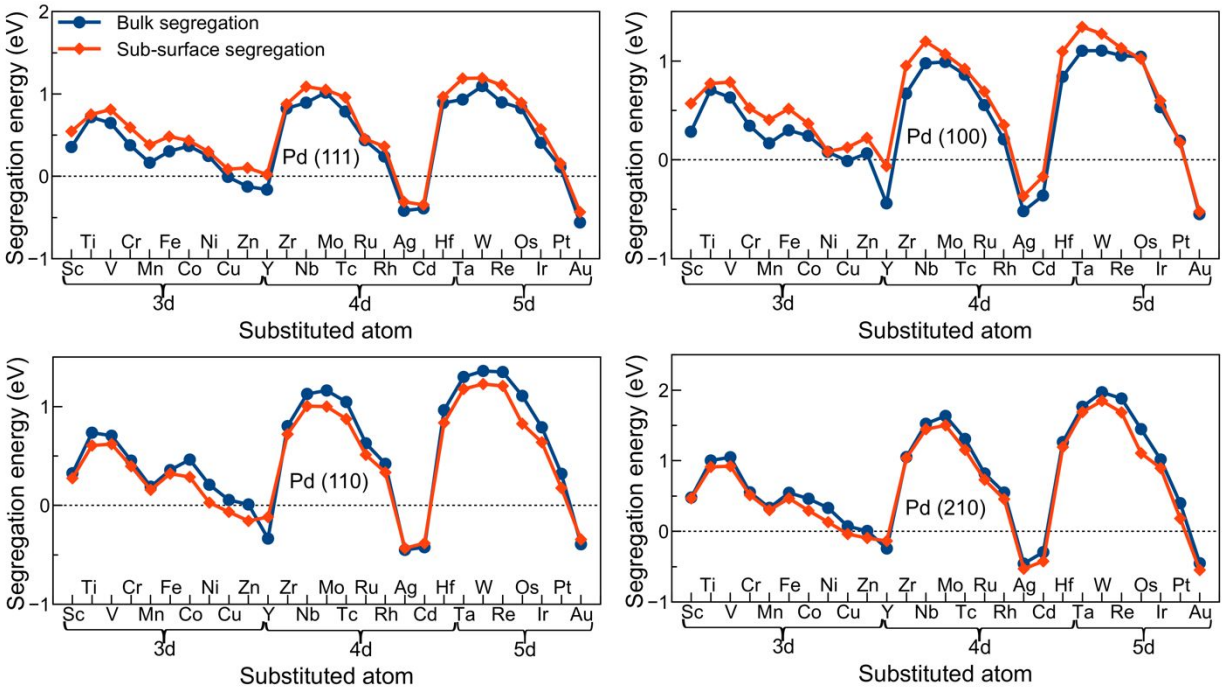

Figure 7. Calculated segregation energies in a Pd host metal involving sub-surface to surface segregation and also bulk to surface segregation. Segregation energies were calculated with Equations (1) and (2).

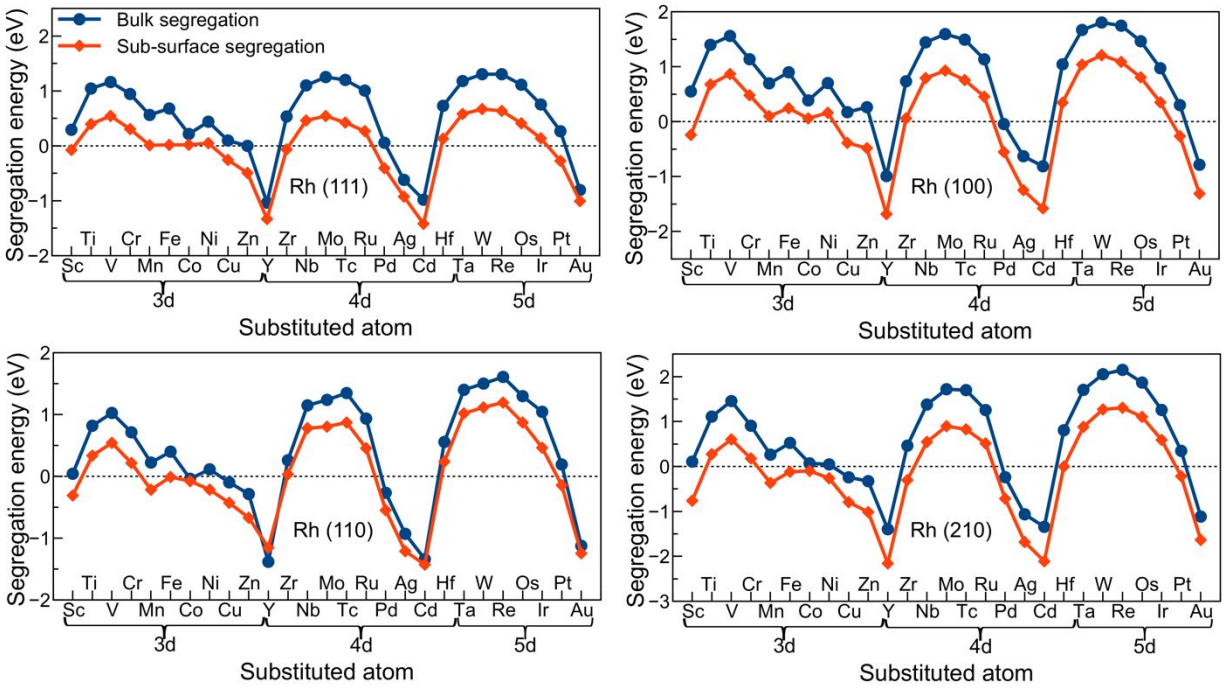

Figure 8. Calculated segregation energies in a Rh host metal involving sub-surface to surface segregation and also bulk to surface segregation. Segregation energies were calculated with Equations (1) and (2).

3.5. Explanation and Analysis of Results

We next sought to develop a mathematical model that could explain and predict surface segregation. Such a model could be used to quickly screen potential alloys without having to run more time-intensive DFT calculations. For instance, many of our DFT calculations took about 18-24 hours to converge, while some calculations took several days to converge. A statistical model would be able to calculate segregation energies in a fraction of this time. Several models have already been published to predict segregation energies. Brejnak and Modrak[79] developed a model to predict segregation energies using properties of pure metals, such as lattice structure, d-band center, d-band width, d-band filling, and atomic volume. They discussed that the sign of the product of $\Delta N\ \alpha_s$ determines whether a dopant atom would segregate to the surface. In the above product, ΔN is the difference between number of d-electrons for alloy components (solute and the solvent) and α_s denotes the surface potential. They used d-band properties of the surface and the bulk simultaneously in order to predict surface segregation, although they did not distinguish between different surfaces. Motivated by this, we also calculated the d-band filling, d-band center, and d-band width for the different surfaces of our host metals that we studied. These results are tabulated in Table S8 in the SI. We plotted d-band properties of Pt along with segregation energy of vanadium as dopant as an example to see if there is a correlation between d-band properties and segregation energy. As it can be seen in Figure S6 in the SI, there is no direct correlation between d-band properties of the host and segregation energies in (111), (100), (110), and (210) surfaces of Pt. This suggests that other properties of the dopants and hosts may be needed for a more complete prediction of segregation energies.

Ruban et al.[28] used Friedel's rectangular state density model[80, 81] to predict segregation energies in transition metal alloys. In their paper they directly compared surface segregation energies of 4d metals calculated using both DFT and their model. Comparing their DFT data with their model indicates how closely the two match. We analyzed their data to calculate an R^2 value of 0.53 between the two data sets, and a root mean square error (RMSE) between the two data sets of 0.41 eV. However, Ruban et al.[28] acknowledged that their model is limited in how it considers the structure of surfaces. A more robust model is needed to better consider segregation behavior between different surfaces.

Another model, based on universal tight-binding (TB) and Friedel's model, developed by Wang and Johnson[23] was used to predict segregation in alloy particles. Wang and Johnson compared segregation energies obtained from their model to their DFT segregation energies in their work. Their model captured the general segregation trends correctly, but there was up to a 3 eV energy difference between their DFT and model results. The R^2 and a root mean square error (RMSE) from comparing their DFT data and model was 0.19 and 0.93 eV respectively.

Yu et al[24]. developed a model to predict segregation energies based on the surface energy, elastic energy, and heat of solution of the impurity and the host metal. Unlike the two previous models which used Friedel's model and tight-binding theory without any regression to fit their data, Yu et al[24], took advantage of linear regression to find coefficients for their utilized parameters. They only modeled Ni (111) as a host metal. We refitted their parameters to our own DFT data (including all host surfaces), and calculated a RMSE of 0.60 eV, R^2 of 0.61, and adjusted R^2 of 0.61 when using their model (with refitted parameters) compared to our DFT data. The drawback of this model however is that it does not predict surface dependent segregation energies since it uses generic experimental surface energies. When we used DFT-calculated surface energies (for the host metals), the RMSE and R^2 were calculated to be 0.50 eV and 0.73, respectively, which was a slight improvement. Unlike a previous model[28], which predicted segregation energies to follow an exact parabola for each facet of Pt with the trend of (210) > (110) > (100) > (111) (contradictory to DFT results), this modified version of Yu et al.'s model captured segregation trends much more realistically. It even captured the oscillatory behavior of the 3d dopants. Segregation energies using this model for Pt as host are plotted in Figure S7 in the SI. This model distinguishes between the (111) surface of Pt and the other surfaces and predicts segregation trends to be (111) > (100) $\approx$ (110) $\approx$ (210). However DFT predicts the following order of segregation energies: (100) > (111) > (210) > (110). Therefore, similar to previous segregation models, the Yu et al.[24] model did not fully capture surface dependent segregation energies.

We therefore developed our own model to predict surface-dependent segregation energies. We took common features of previous models to derive the model shown in Equation (3). Our model uses d-band width (W^B), d-band filling of the dopant (N_B), coordination number in the

surface (Z_s) and in the bulk (Z_b), a term representing the elastic energy release ($\left[\left(\frac{r_B}{r_A}\right)^3 - 1\right]^2 r_A^3$), and surface energy difference of the host and the dopant ($E^B_{surface} - E^A_{surface}$). This model takes elements of Ruban et al[28] (coordination numbers and d-band properties), but also adds in features from Yu et al[24] (difference in surface energies and elastic energy). The model also includes adjustable parameters, which allows more flexibility. This model was directly fitted to all our DFT data (all Pt, Ir, Pd, Rh host surfaces), and is given in Equation (3), where the β coefficients are the fitted parameters. The model gave a RMSE of 0.43 eV and an adjusted R^2 of 0.77. The exact parameters of the model can be found in the SI.

$$E^{B\to A}_{segregation} = \beta_0 + \beta_1 W^B + \beta_2 N_B + \beta_3\left(E^B_{surface} - E^A_{surface}\right) + \beta_4\left[\left(\frac{r_B}{r_A}\right)^3 - 1\right]^2 r_A^3 + \beta_5\left[1 - \left(\frac{Z_b}{Z_s}\right)^{\frac{1}{2}}\right] \quad (3)$$

Further explanation of all the parameters and how we developed this model can be found in the SI. Figure 9 shows how our DFT data compares to our model. Table 1 shows a summary of how our model compares to our DFT data, as well as some other models in the literature. Overall, our model captures the features of the DFT model quite well.

The large adjusted R^2 value of 0.77 and low $RMSE$ of 0.43 eV indicate the accuracy of our model. The largest difference between the DFT data and our model belongs to Ir as the host with a difference of 1.62 eV. The comparison between segregation energies calculated with DFT and our model for (111), (100), (110), and (210) surfaces of Pt is depicted in Figure 9. As is evident from the figure, our model mirrors the DFT results well. Our model is able to describe surface-dependent segregation, a feature previously not included in segregation models. The corresponding figures for Ir, Pd, and Rh can be found in Figures S8-S10. Our model takes into account d-band properties of the dopant (d-band filling and d-occupation number), surface energy of the host and dopant, atomic radii of the host and dopant, and also coordination numbers in the bulk and at the surface. All these parameters combined give a surface dependent segregation model that agrees well with DFT. Previous models did not consider all these parameters at the same time and as a result were not able to achieve such good agreement with DFT, especially for different surfaces.

One particular danger is using a model for predictions that the model was not intended for or incapable of making. To test our model we compared DFT calculations of the Pt (211) surface

with predictions of our model to determine how our model may perform for surfaces outside the training set. Table S10 shows such results, and indicates that our model does very well in predicting segregation energies for this surface. Thus our model is robust in making predictions for other surfaces of the host metals. We will acknowledge that the β parameters were fitted using a select number of transition metal hosts, and that different hosts may require re-fitting to determine relevant parameters. We expect however that the same features (e.g. d-band properties, surface energies, etc.) will be relevant for such hosts.

Table 1. Comparison between various models to predict surface segregation and DFT data. In the case of Ruban et al.[28] and Wang et al.[23] the models were compared with the DFT data in the original papers, while for Yu et al.[24] and our model our own DFT data was used for comparison.

Model	R^2	Adjusted R^2	RMSE (eV)	Largest Difference (eV)	Smallest Difference (eV)
Ruban et al.[28]	0.53	-	0.41	1.32	0.01
Wang et al.[23]	0.19	-	0.93	3.16	0.00
Yu et al.[24]	0.61	0.61	0.60	1.74	0.00
Our Model	0.77	0.77	0.43	1.62	0.00

Our model shows good agreement with DFT calculations, but such a model should be more than just a highly fitted model with non-relevant features. The model should reflect the chemistry and physics of segregation processes, and materials involved. The model should also help explain what underlying physical features determine segregation phenomena. Our model includes several features; interplay between the various forces/influences that these features represent determines to which degree segregation will occur between two metals. The model includes d-band filling and d-occupation number. The electronic properties of the dopant metal are surely important for segregation, as the electronic structure determines the strength on bonding interactions between the dopant metal and host metal. Metals with wide d-bands and larger number of d electrons have more opportunities to form favorable bonds with the host metal. The surface energy difference between the host and dopant metal is also one of the parameters. The surface energy difference is

important because it indicates the relative preference for such metals to form structures with undercoordinated atoms, i.e. surfaces. When the dopant metal more readily forms a surface than the host metal ($E^B_{surface} > E^A_{surface}$), this is indicative that such dopant metals are more stable in undercoordinated environments, and in the host metal may more readily migrates to the surface, or may segregate. Surface energy is related to the related to the number of unfilled orbitals: early and late transition metals tend to have lower surface energies than mid transition metals[24] which reflects the number of unfilled d orbitals, and hence the desire of such atoms for forming bonds.

The relative atomic radii of both the host and dopant metal are also part of the model. If the host metal is much smaller than the dopant metal (r_B/r_A large), this adds strain to the alloy and favors segregation, which our model reveals. The relative coordination numbers of the host metal in the surface and at the surface are also included in the model. The model includes the term $1-(Z_b/Z_s)^{½}$. Different surfaces will have different coordination numbers, and segregation is less likely to occur at surfaces with smaller coordination numbers since any dopant atoms on the surface would be less stable, having less coordination, than in the bulk. In summary, the size, coordination, and electronic properties of the host/dopants all play important roles in determining whether segregation will occur, as reflected by our model.

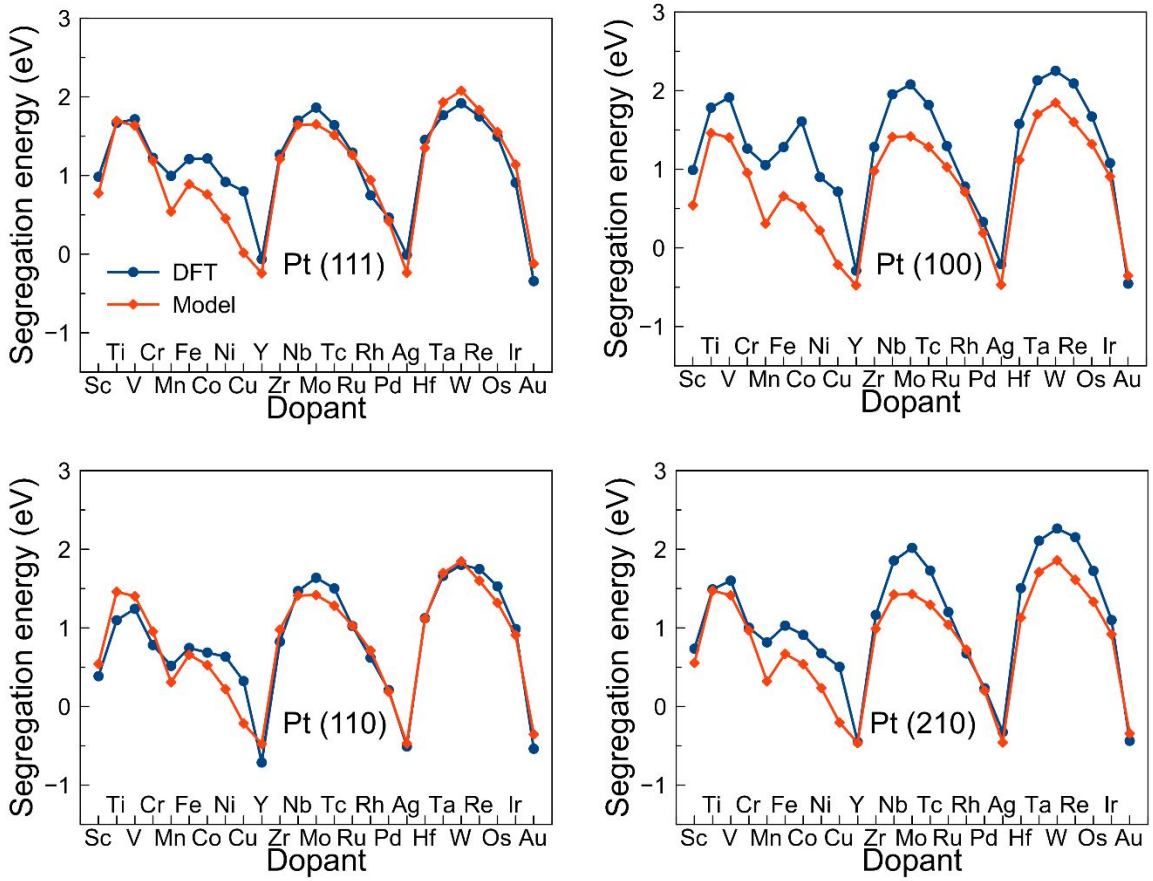

Figure 9. Comparison between segregation energies of various dopants in the (111), (100), (110), and (210) surfaces of Pt obtained with DFT and our developed model.

4. Conclusions

We calculated segregation energies using DFT for alloys involving Pt, Pd, Ir, and Rh as host and transition metals as dopants. Segregation energies may very well depend on the exposed surface, which is what we show in our results. For instance, with Pt as the host and 3d transition metals as dopants the segregation energies follow the trend of: (100) > (111) > (210) > (110). However, for Pt as the host and 4d and 5d transition metals as dopants the following trend was observed: (100) $\approx$ (210) > (111) > (110). In general, early and late transition metals segregate more and have more negative segregation energies, while mid-transition metals possess positive segregation energies and do not tend to segregate. An oscillatory segregation behavior is observed in 3d transition metals. We also calculated segregation energies in other hosts including Ir, Rh,

and Pd. When considering all the (111), (100), (110), and (210) surfaces, the general trend in the segregation energies for the various hosts is Pt > Rh > Pd > Ir. We also compared bulk and sub-surface segregation energies (segregation from the bulk or from the sub-layer) and found the segregation trends to be very similar between the two segregation processes.

We further developed a statistical model which predicts segregation of the transition metal dopants. This model used several parameters, including d-band width and d-band filling of the dopant, surface energies of the host and impurity, an elastic energy release term, and coordination number. This model is able to predict surface-dependent segregation, and is in good agreement with the DFT data. Our model is an improvement on previous models in that it can distinguish segregation at different host surfaces, and has high accuracy. Such results are important for predicting and understanding the stability of different metal alloy crystals/particles, and will allow for faster screening of potential alloys.

Acknowledgements

We thank the National Science Foundation (CBET 1705830) for funding. Computational resources were provided by Worcester Polytechnic Institute and XSEDE.

References

1. F. Y. Cheng, H. Ma, Y. M. Li and J. Chen, *Inorg Chem*, 2007, **46**, 788-794.
2. S. Akbayrak, Y. Tonbul and S. Ozkar, *Appl Catal B-Environ*, 2016, **198**, 162-170.
3. P. Biloen, F. M. Dautzenberg and W. M. H. Sachtler, *Journal of Catalysis*, 1977, **50**, 77-86.
4. V. M. Gryaznov, M. M. Ermilova, L. S. Morozova, N. V. Orekhova, V. P. Polyakova, N. R. Roshan, E. M. Savitsky and N. I. Parfenova, *J Less-Common Met*, 1983, **89**, 529-535.
5. A. Rochefort, F. Lepeltier and J. P. Boitiaux, *Journal of Catalysis*, 1992, **138**, 482-490.
6. R. Burch, *Journal of Catalysis*, 1981, **71**, 348-359.
7. R. Burch and L. C. Garla, *Journal of Catalysis*, 1981, **71**, 360-372.
8. E. Antolini, *Journal of Power Sources*, 2007, **170**, 1-12.
9. H. R. Colon-Mercado and B. N. Popov, *Journal of Power Sources*, 2006, **155**, 253-263.
10. Y. Y. Shao, G. P. Yin and Y. Z. Gao, *Journal of Power Sources*, 2007, **171**, 558-566.
11. S. S. Zhang, X. Z. Yuan, J. N. C. Hin, H. J. Wang, K. A. Friedrich and M. Schulze, *Journal of Power Sources*, 2009, **194**, 588-600.
12. R. Ferrando, J. Jellinek and R. L. Johnston, *Chem Rev*, 2008, **108**, 845-910.
13. P. A. Dowben and A. Miller, *Surface Segregationphenomena*, CRC Press1990.
14. G. F. Wang, M. A. Van Hove, P. N. Ross and M. I. Baskes, *Prog Surf Sci*, 2005, **79**, 28-45.
15. L. Peng, E. Ringe, R. P. Van Duyne and L. D. Marks, *Physical Chemistry Chemical Physics*, 2015, **17**, 27940-27951.
16. Y. G. Ma and P. B. Balbuena, *Surface Science*, 2008, **602**, 107-113.
17. K. J. J. Mayrhofer, V. Juhart, K. Hartl, M. Hanzlik and M. Arenz, *Angew Chem Int Edit*, 2009, **48**, 3529-3531.
18. J. R. Kitchin, J. K. Norskov, M. A. Barteau and J. G. Chen, *J Chem Phys*, 2004, **120**, 10240-10246.
19. V. R. Stamenkovic, B. Fowler, B. S. Mun, G. F. Wang, P. N. Ross, C. A. Lucas and N. M. Markovic, *Science*, 2007, **315**, 493-497.
20. G. F. Wang, M. A. Van Hove, P. N. Ross and M. I. Baskes, *J Chem Phys*, 2005, **122**.
21. G. E. Ramirez-Caballero and P. B. Balbuena, *Chem Phys Lett*, 2008, **456**, 64-67.
22. O. M. Lovvik, *Surface Science*, 2005, **583**, 100-106.
23. L. L. Wang and D. D. Johnson, *Journal of the American Chemical Society*, 2009, **131**, 14023-14029.
24. Y. L. Yu, W. Xiao, J. W. Wang and L. G. Wang, *Phys Chem Chem Phys*, 2016, **18**, 26616-26622.
25. F. Calvo, *Physical Chemistry Chemical Physics*, 2015, **17**, 27922-27939.
26. A. U. Nilekar, A. V. Ruban and M. Mavrikakis, *Surface Science*, 2009, **603**, 91-96.
27. A. V. Ruban and H. L. Skriver, *Comp Mater Sci*, 1999, **15**, 119-143.
28. A. V. Ruban, H. L. Skriver and J. K. Norskov, *Phys Rev B*, 1999, **59**, 15990-16000.
29. Y. H. Zhang, Z. Y. Duan, C. Xiao and G. F. Wang, *Surface Science*, 2011, **605**, 1577-1582.
30. S. Chen, P. J. Ferreira, W. C. Sheng, N. Yabuuchi, L. F. Allard and Y. Shao-Horn, *Journal of the American Chemical Society*, 2008, **130**, 13818-13819.
31. H. Guesmi, C. Louis and L. Delannoy, *Chem Phys Lett*, 2011, **503**, 97-100.
32. G. Barcaro, A. Fortunelli, M. Polak and L. Rubinovich, *Nano Lett*, 2011, **11**, 1766-1769.
33. G. E. Ramírez-Caballero, Y. Ma, R. Callejas-Tovar and P. B. Balbuena, *Physical Chemistry Chemical Physics*, 2010, **12**, 2209-2218.
34. H.-C. Tsai, T. H. Yu, Y. Sha, B. V. Merinov, P.-W. Wu, S.-Y. Chen and W. A. Goddard, *The Journal of Physical Chemistry C*, 2014, **118**, 26703-26712.
35. Y. Gauthier, R. Baudoing and J. Jupille, *Phys Rev B*, 1989, **40**, 1500-1510.
36. Y. Gauthier, R. Baudoing, M. Lundberg and J. Rundgren, *Phys Rev B*, 1987, **35**, 7867-7878.

37. J. Luyten, M. Schurmans, C. Creemers, B. S. Bunnik and G. J. Kramer, *Surface Science*, 2007, **601**, 1668-1676.
38. A. Matveev, *Journal of Surface Investigation. X-ray, Synchrotron and Neutron Techniques*, 2013, **7**, 774-783.
39. L. Rubinovich and M. Polak, *Physical Review B*, 2009, **80**, 045404.
40. Y. K. Shin, L. L. Gai, S. Raman and A. C. T. van Duin, *J Phys Chem A*, 2016, **120**, 8044-8055.
41. D. Tomanek, A. A. Aligia and C. A. Balseiro, *Phys Rev B*, 1985, **32**, 5051-5056.
42. G. Treglia and B. Legrand, *Phys Rev B*, 1987, **35**, 4338-4344.
43. S. M. Foiles, M. I. Baskes and M. S. Daw, *Phys Rev B*, 1986, **33**, 7983-7991.
44. R. M. Anderson, L. Zhang, J. A. Loussaert, A. I. Frenkel, G. Henkelman and R. M. Crooks, *Acs Nano*, 2013, **7**, 9345-9353.
45. Z. Y. Duan and G. F. Wang, *J Phys-Condens Mat*, 2011, **23**.
46. P. L. Hansen, A. M. Molenbroek and A. V. Ruban, *J Phys Chem B*, 1997, **101**, 1861-1868.
47. L. T. Roling, T. S. Choksi and F. Abild-Pedersen, *Nanoscale*, 2019, **11**, 4438-4452.
48. M. Frigo and S. G. Johnson, *P Ieee*, 2005, **93**, 216-231.
49. J. Hutter, M. Iannuzzi, F. Schiffmann and J. VandeVondele, *Wires Comput Mol Sci*, 2014, **4**, 15-25.
50. G. Lippert, J. Hutter and M. Parrinello, *Mol Phys*, 1997, **92**, 477-487.
51. J. VandeVondele and J. Hutter, *J Chem Phys*, 2003, **118**, 4365-4369.
52. J. VandeVondele, M. Krack, F. Mohamed, M. Parrinello, T. Chassaing and J. Hutter, *Comput Phys Commun*, 2005, **167**, 103-128.
53. J. VandeVondele and J. Hutter, *J Chem Phys*, 2007, **127**.
54. S. Goedecker, M. Teter and J. Hutter, *Phys Rev B*, 1996, **54**, 1703-1710.
55. M. Krack, *Theor Chem Acc*, 2005, **114**, 145-152.
56. J. Courtois, W. Du, E. Wong, X. Teng and N. A. Deskins, *Applied Catalysis A: General*, 2014, **483**, 85-96.
57. J. P. Perdew, K. Burke and M. Ernzerhof, *Phys Rev Lett*, 1996, **77**, 3865-3868.
58. F. Tran, R. Laskowski, P. Blaha and K. Schwarz, *Physical Review B*, 2007, **75**, 115131.
59. V. Polo, E. Kraka and D. Cremer, *Molecular Physics*, 2002, **100**, 1771-1790.
60. P. Haas, F. Tran and P. Blaha, *Physical Review B*, 2009, **79**, 085104.
61. P. Janthon, S. Luo, S. M. Kozlov, F. Viñes, J. Limtrakul, D. G. Truhlar and F. Illas, *Journal of Chemical Theory and Computation*, 2014, **10**, 3832-3839.
62. R. Brako, D. Sokcevic, P. Lazic and N. Atodiresei, *New J Phys*, 2010, **12**.
63. P. Haas, F. Tran and P. Blaha, *Phys Rev B*, 2009, **79**.
64. P. J. Feibelman, B. Hammer, J. K. Norskov, F. Wagner, M. Scheffler, R. Stumpf, R. Watwe and J. Dumesic, *J Phys Chem B*, 2001, **105**, 4018-4025.
65. J. A. Boscoboinik, C. Plaisance, M. Neurock and W. T. Tysoe, *Phys Rev B*, 2008, **77**.
66. X. Z. Ke, G. J. Kramer and O. M. Lovvik, *J Phys-Condens Mat*, 2004, **16**, 6267-6277.
67. O. M. Lovvik and R. A. Olsen, *J Alloy Compd*, 2002, **330**, 332-337.
68. O. M. Lovvik and R. A. Olsen, *J Chem Phys*, 2003, **118**, 3268-3276.
69. C. G. Sonwane, J. Wilcox and Y. H. Ma, *J Phys Chem B*, 2006, **110**, 24549-24558.
70. O. Dieguez and N. Marzari, *Phys Rev B*, 2009, **80**.
71. F. Frechard, R. A. van Santen, A. Siokou, J. W. Niemantsverdriet and J. Hafner, *J Chem Phys*, 1999, **111**, 8124-8130.
72. O. R. Inderwildi, D. Lebiedz, O. Deutschmann and J. Warnatz, *J Chem Phys*, 2005, **122**.
73. J. R. Chelikowsky, *Surface Science*, 1984, **139**, L197-L203.
74. S. Mukherjee and J. Moran-Lopez, *Surface Science*, 1987, **188**, L742-L748.
75. A. P. Sutton, *Electronic structure of materials*, Clarendon Press1993.
76. P. H. T. Philipsen and E. J. Baerends, *Physical Review B*, 1996, **54**, 5326-5333.

77. R. Zeller, in *Computational Nanoscience: Do It Yourself*, eds. J. Grotendorst, S. Blugel and D. Marx, John von Neumann Institute for Computing, Julich2006, vol. 31, pp. 419-445.
78. A. d. Niessen, F. De Boer, R. Boom, P. De Chatel, W. Mattens and A. Miedema, *Calphad*, 1983, **7**, 51-70.
79. M. Brejnak and P. Modrak, *Surface Science*, 1991, **247**, 215-221.
80. F. Cyrot-Lackmann, *Advances in Physics*, 1967, **16**, 393-400.
81. J. Friedel, *Ann Phys-Paris*, 1976, **1**, 257-307.